DØ Note 4731-CONF v2.3

Study of Flavor Changing Neutral Current Charm Decays and Observation of $D_s^+ \to \phi\pi^+ \to \pi^+\mu^+\mu^-$

The DØ Collaboration
URL: http://www-d0.fnal.gov
Contact Person for This Analysis: bcasey@fnal.gov

(Dated: March 13, 2005)

We study the flavor changing neutral current process $c \to u\mu^+\mu^-$ using a 508 pb^{-1} data sample of $p\bar{p}$ collisions at $\sqrt{s} = 1.96$ TeV recorded by the DØ detector operating at the Fermilab Tevatron. We observe the $D_s^+ \to \phi\pi^+ \to \pi^+\mu^+\mu^-$ final state with a significance above background greater than 7 standard deviations. We measure $13.2^{+5.6}_{-4.9}$ $D^+ \to \pi^+\mu^+\mu^-$ events in the same $\mu^+\mu^-$ invariant mass range with a significance of 2.7 standard deviations above background and set a limit on the ratio of branching fractions of $\mathcal{B}(D^+ \to \phi\pi^+ \to \pi^+\mu^+\mu^-)/\mathcal{B}(D_s^+ \to \phi\pi^+ \to \pi^+\mu^+\mu^-) < 0.28$ at the 90% confidence level. Using the measured values of the $D_s^+ \to \phi\pi^+$ and $\phi \to \mu^+\mu^-$ branching fractions we convert this to a limit on the branching fraction of $\mathcal{B}(D^+ \to \phi\pi^+ \to \pi^+\mu^+\mu^-) < 3.1 \times 10^{-6}$ at the 90% confidence level. This is the first step in a program to limit new phenomena contributions in the up quark sector by searching for an excess in events where the $\mu^+\mu^-$ system is not produced through a resonance.

INTRODUCTION

Flavor changing neutral current (FCNC) decays are forbidden at tree level in the standard model (SM) and proceed via higher order penguin or box diagrams. Many extensions of the SM allow for tree level diagrams or alternative loop diagrams for FCNC that could significantly alter the decay rate with respect to SM expectations. The excellent agreement between observed FCNC processes involving down type charge $-1/3$ quarks such as $b \to s\gamma$, $b \to sl^+l^-$, and $K \to \pi\nu\bar{\nu}$ with SM expectations have been used to set strict limits on new phenomena [1–3]. However, there are several scenarios of new phenomena such as SUSY R parity violation in a single coupling scheme where R parity could be violated in the up sector or the down sector but not both [3]. Scenarios of this nature motivate the study of FCNC charm meson decays.

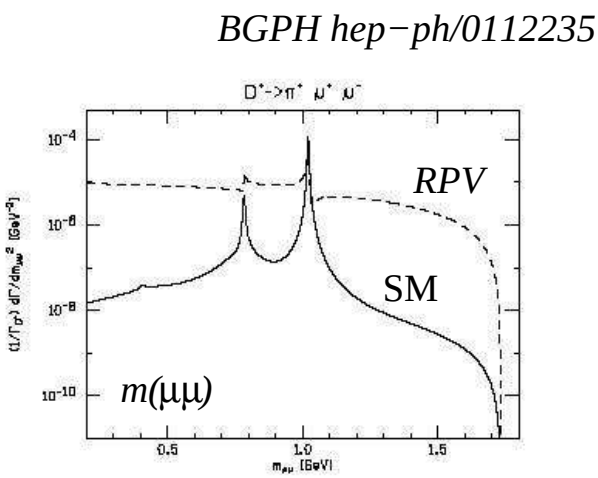

FIG. 1: Predicted dimuon invariant mass spectrum for $D^+ \to \pi^+\mu^+\mu^-$ transitions reproduced from Ref. [5]. The solid line is the Standard Model expectation. The dashed line is the possible enhancement due to R parity violation.

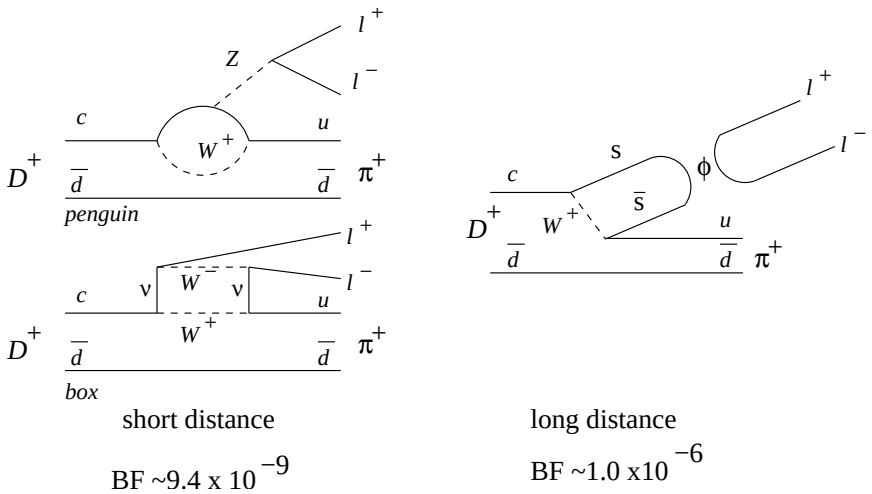

FIG. 2: Feynman diagrams for the $D^+ \to \pi^+\mu^+\mu^-$ decay showing the short distance SM box and penguin decay mechanisms as well as the long distance decay mechanism via an intermediate vector resonance. The expected branching fractions are taken from Ref. [6].

The predicted dimuon invariant mass spectrum [5] for the $D^+ \to \pi^+\mu^+\mu^-$ final state is displayed in Fig. 1 including the expected enhancement due to R parity violation in the up quark sector. Due to GIM suppression, the SM rates for FCNC charm decays vanish in the limit of SU(3) symmetry. The inclusive rates of decays such as $D^+ \to \pi^+l^+l^-$ [4] are therefore expected to be dominated by long distance contributions where the dilepton system is produced via intermediate strong resonances such as the ϕ or the ω [5, 6] as illustrated in Fig. 2. Just as the decay $B^+ \to$

$J/\psi K^+ \to K^+ l^+ l^-$ played a crucial role in benchmarking the studies of $b \to s l^+ l^-$ transitions, the observation of the decay $D_s^+ \to \phi\pi^+ \to \pi^+ l^+ l^-$ is an essential first step in the study of $c \to u l^+ l^-$ transitions.

In this Note we report a study of FCNC charm decays including the observation of the decay $D_s^+ \to \phi\pi^+ \to \pi^+\mu^+\mu^-$. The study uses a 508 pb^{-1} data set of $p\bar{p}$ collisions at $\sqrt{s} = 1.96$ TeV recorded by the DØ detector operating at the Fermilab Tevatron. Similar studies have been performed by other experiments with the most stringent limits on three body FCNC charm decays being set by FOCUS [7].

PROCEDURE

Detector and Trigger

The DØ detector is a general purpose spectrometer and calorimeter [8]. Charged particles are reconstructed using a silicon vertex tracker and a scintillating fiber tracker located inside a superconducting solenoid coil that provides a 2 T magnetic field. Photons and electrons are reconstructed using the inner region of a liquid argon calorimeter optimized for electromagnetic shower detection. Jet reconstruction and electron identification are further augmented with the outer region of the calorimeter optimized for hadronic shower detection. Muons are reconstructed using a spectrometer consisting of magnetized iron toroids and three super layers of proportional tubes and plastic trigger scintillators located outside the calorimeter.

The DØ trigger is based on a three tier system. The level 1 and 2 muon triggers rely on energy deposited in the muon spectrometer and fast reconstruction of muon tracks. The level 3 trigger performs fast reconstruction of the entire event allowing for further muon identification algorithms, matching of muon candidates to tracks reconstructed in the central tracking system, and requirements on the z position of the primary vertex. We only consider events that were triggered by a suite of dimuon triggers.

D Reconstruction

The analysis requirements are determined using Pythia [9] Monte Carlo (MC) to model both $c\bar{c}$ and $b\bar{b}$ production and fragmentation. The EvtGen [10] MC is used to decay prompt D mesons and secondary D mesons from B meson decay into the $\phi\pi^+$ and $\pi^+\mu^+\mu^-$ intermediate and final states. The prompt fraction is set to the measured value at the Tevatron [11]. The detector response is modeled using a GEANT [12] based MC. Backgrounds are modeled using data in the mass sideband regions of $1.4 < m(\pi\mu^+\mu^-) < 1.75$ GeV/c^2 and $2.05 < m(\pi\mu^+\mu^-) < 2.4$ GeV/c^2.

Muon candidates are required to have segments reconstructed in at least two of the muon system super layers and be associated to a track reconstructed with hits in both the silicon and fiber trackers. The muon momentum determined by the muon spectrometer is replaced by the momentum of the associated track. We require the muon transverse momentum p_T be greater than 2 GeV/c and the total momentum p be above 3 GeV/c. The dimuon system is formed by combining two oppositely charged muon candidates that are associated with the same track jet [13] and the same primary vertex, form a well reconstructed vertex, and have an invariant mass $m(\mu^+\mu^-)$ below 2 GeV/c^2. For the initial search for the long distance component to the $\mu^+\mu^-$ system, we require $0.96 < m(\mu^+\mu^-) < 1.06$ GeV/c^2 and redetermine the $\mu^+\mu^-$ momentum with a ϕ mass constraint imposed. The dimuon mass distribution in the region of the ϕ, ω, and ρ resonances is shown in Fig. 3.

Candidate $D_{(s)}^+$ mesons are formed by combining the dimuon system with a track that is associated with the same track jet and primary vertex as the dimuon system, has hits in both the silicon and fiber trackers, and $p_T > 0.18$ GeV/c. The invariant mass of the three body system must be in the range 1.3 GeV/c^2 $< m(\mu^+\mu^-\pi^+) <$ 2.5 GeV/c^2. The three particles must form a well reconstructed vertex and the flight direction must be consistent with a particle originating from the primary vertex.

The above selection criteria yields an average of 3.3 candidates per event in events where at least one candidate is reconstructed. We choose the candidate with the minimum value of

$$\mathcal{M} = \chi^2_{\rm vtx} + (1/p_T(\pi))^2 + \Delta R^2_\pi,$$

where $\chi^2_{\rm vtx}$ is the three particle vertex χ^2, ΔR_π is the distance in η, ϕ space between the π and the $\mu^+\mu^-$ system, and the π transverse momentum is in units of GeV/c. This selects the correct candidate in 90% of MC events. The above combination was found to give the highest efficiency as compared to using different weights for the different variables. The $m(\pi^+\mu^+\mu^-)$ distributions for MC and data after the above selection criteria are shown in Fig. 4.

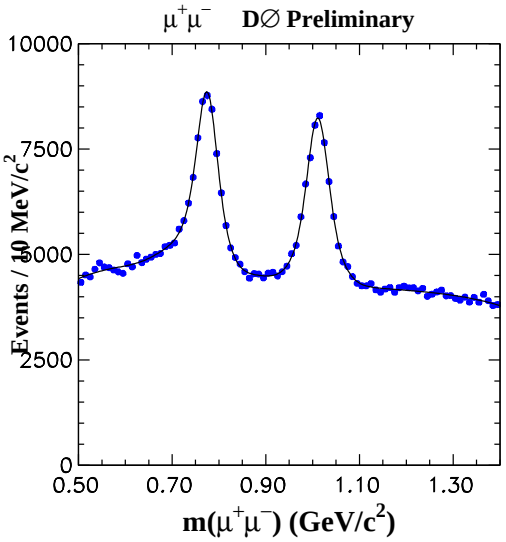

FIG. 3: The inclusive $m(\mu^+\mu^-)$ invariant mass spectrum for the 508 pb^{-1} DØ data sample. The solid line is a fit to the distribution that includes components for $\phi \to \mu^+\mu^-$, $\omega \to \mu^+\mu^-$, and $\rho \to \mu^+\mu^-$ as well as combinatoric background.

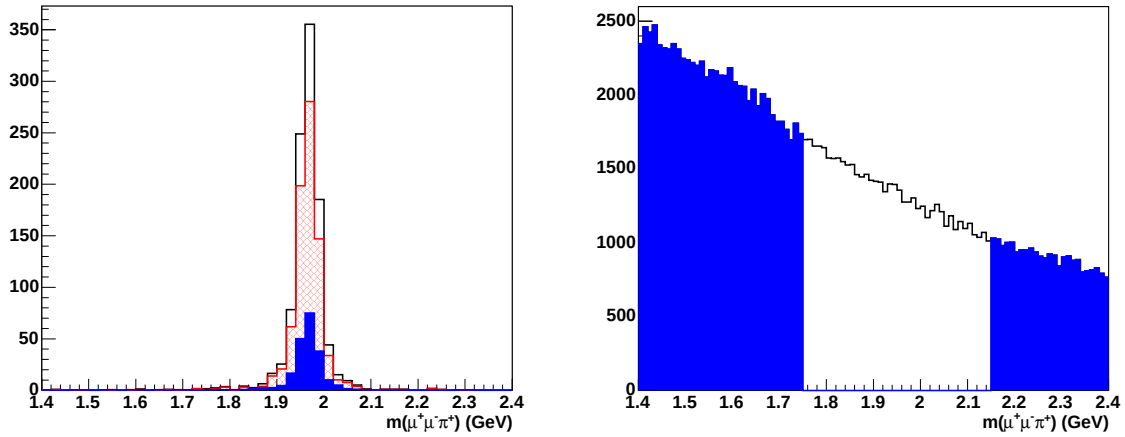

FIG. 4: The $m(\mu^+\mu^-\pi^+)$ distribution for $D_s^+ \to \phi\pi^+ \to \pi^+\mu^+\mu^-$ signal MC (left). The hatched red histogram is the prompt component; the solid blue histogram is the $B \to D_s$ component; the open black histogram is the sum of the two components. The right histogram is the distribution in the 508 pb^{-1} data sample after applying the D selection requirements described in the text. The blue solid region signifies the sideband used to model the background for the background suppression variables.

Background Suppression

Backgrounds are reduced using four variables (Fig. 5): The Isolation is defined as

$$\mathcal{I}_D = p(D)/\sum p_{\rm cone}$$

where the sum is over tracks in a cone of $\Delta R < 1$ centered on the D meson. The tracks are also required to have $p_T > 200$ MeV, at least three hits on the track, and have a z coordinate within 5 cm of the D meson; the transverse flight length significance $\mathcal{S}_D$ defined as the transverse distance of the reconstructed D vertex from the primary vertex normalized to the error in the primary and D vertex measurements; the collinearity angle Θ_D defined as the angle between the D momentum vector and the position vector pointing from the primary to the secondary vertex; finally the significance ratio $\mathcal{R}_\mathcal{S}$ defined as the ratio of the π^+ impact parameter significance to $\mathcal{S}_D$. The variables are displayed in Figures 6 through 9 for signal MC and sideband data.

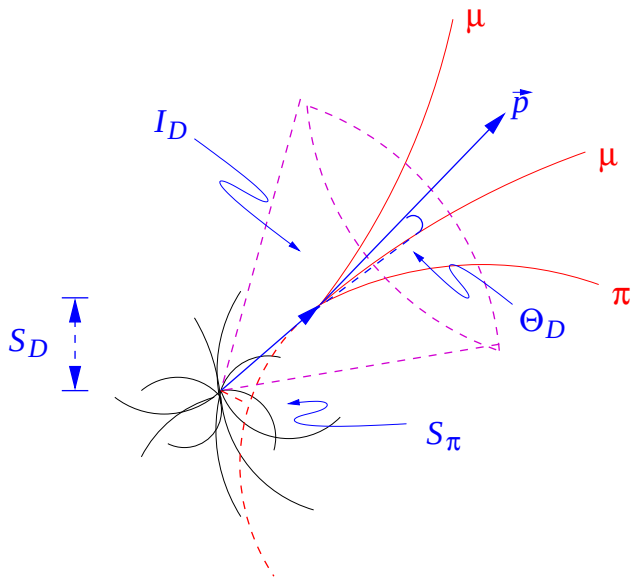

FIG. 5: Representation of the background suppression variables described in the text.

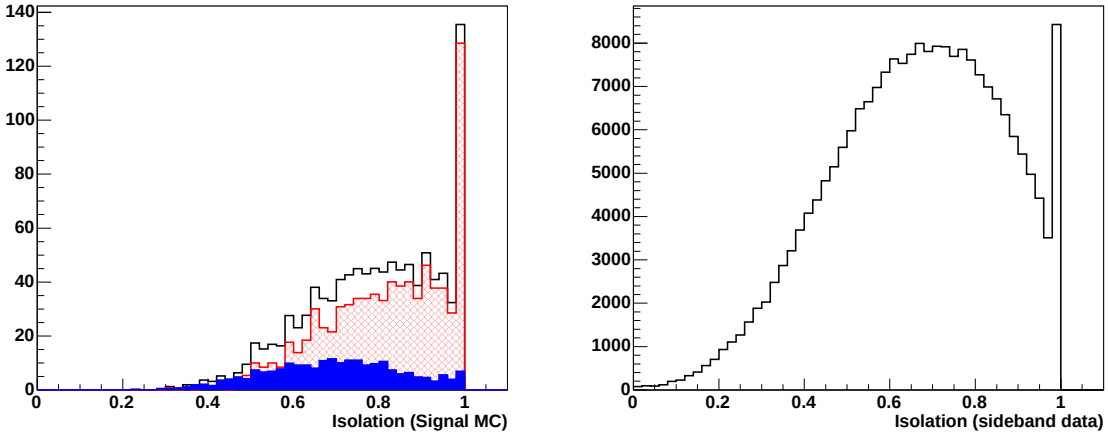

FIG. 6: The isolation variable, $\mathcal{I}_D$. The distribution on the left is $D_s \to \phi\pi \to \pi\mu^+\mu^-$ signal MC. The hatched red histogram is the prompt component; the solid blue histogram is the $B \to D_s$ component; the open black histogram is the sum of the two components. The distribution on the right is D candidates in the 508 pb^{-1} data sample in the D mass sideband regions $1.4 < m(\pi\mu^+\mu^-) < 1.75$ GeV/c^2 and $2.05 < m(\pi\mu^+\mu^-) < 2.4$ GeV/c^2.

We first require the following criteria that are close to 100% efficient for signal: $\Theta_D < 0.2$, $\mathcal{R}_\mathcal{S} < 1.5$, and $\mathcal{S}_D < 100$. We then combine the four background suppression variables into a single likelihood. To a good approximation, $\mathcal{I}_D$ is independent of the other three variables. The remaining three variables are independent for candidates with well separated secondary vertices but become highly correlated near the interaction region as displayed in Figure 10. We therefore construct the following likelihoods:

$$\mathcal{L} = \mathcal{L}(\mathcal{I}_D) \times \mathcal{L}(\mathcal{S}_D, \Theta_D, \mathcal{R}_\mathcal{S}) \qquad \mathcal{S}_D < 20$$

$$\mathcal{L} = \mathcal{L}(\mathcal{I}_D) \times \mathcal{L}(\mathcal{S}_D) \times \mathcal{L}(\Theta_D) \times \mathcal{L}(\mathcal{R}_\mathcal{S}) \quad \mathcal{S}_D \geq 20$$

The one dimensional probability density functions (PDFs) are parameterized functions determined from signal MC and sideband data. The three-dimensional PDFs are three-dimensional histograms. The normalized likelihood ratio,

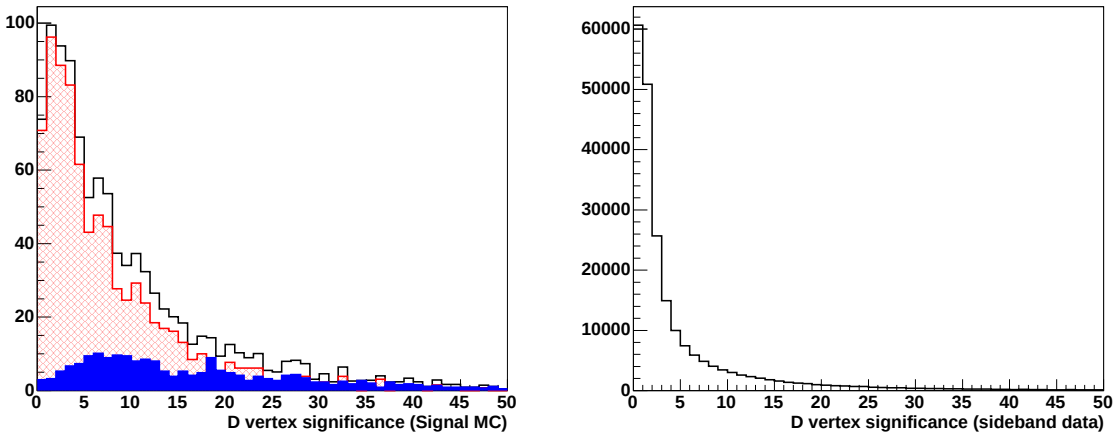

FIG. 7: The significance variable, $\mathcal{S}_D$. The distribution on the left is $D_s \to \phi\pi \to \pi\mu^+\mu^-$ signal MC. The hatched red histogram is the prompt component; the solid blue histogram is the $B \to D_s$ component; the open black histogram is the sum of the two components. The distribution on the right is D candidates in the 508 pb^{-1} data sample in the D mass sideband regions $1.4 < m(\pi\mu^+\mu^-) < 1.75$ GeV/c^2 and $2.05 < m(\pi\mu^+\mu^-) < 2.4$ GeV/c^2.

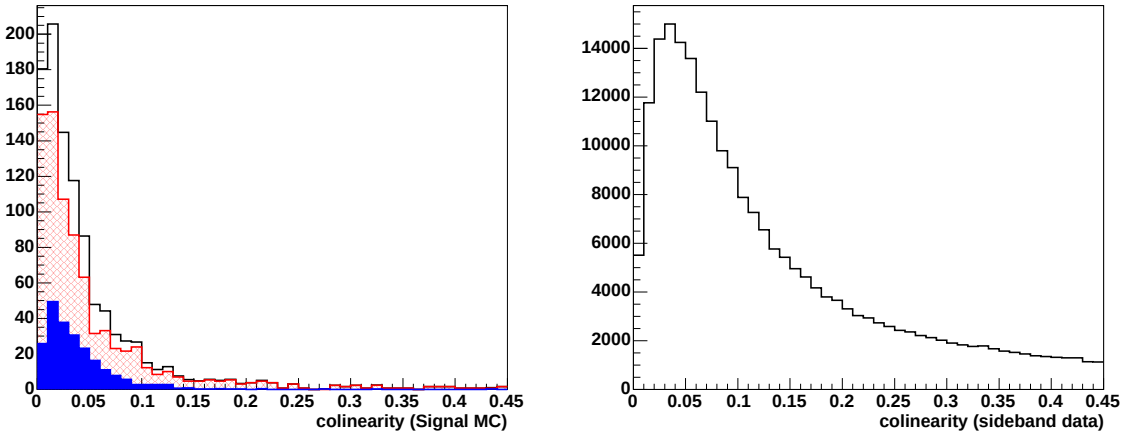

FIG. 8: The collinearity angle variable, Θ_D. The distribution on the left is $D_s \to \phi\pi \to \pi\mu^+\mu^-$ signal MC. The hatched red histogram is the prompt component; the solid blue histogram is the $B \to D_s$ component; the open black histogram is the sum of the two components. The distribution on the right is D candidates in the 508 pb^{-1} data sample in the D mass sideband regions $1.4 < m(\pi\mu^+\mu^-) < 1.75$ GeV/c^2 and $2.05 < m(\pi\mu^+\mu^-) < 2.4$ GeV/c^2.

d defined as

$$d = \frac{\mathcal{L}(\text{signal})}{\mathcal{L}(\text{signal}) + \mathcal{L}(\text{background})}$$

is plotted in Fig. 11.

We determine the requirement on the likelihood ratio by tuning on $\epsilon_S/\sqrt{\epsilon_B}$ where ϵ_S is the signal efficiency including both prompt and $B \to D$ components properly weighted, and ϵ_B is the background efficiency taken from sideband data. This study yields an optimal requirement of $d > 0.9$.

Signal Extraction

Figure 12 shows the $m(\pi^+\mu^+\mu^-)$ mass spectrum for events passing all requirements in the region $0.96 < m(\mu^+\mu^-) < 1.06$ GeV/c^2 and $1.4 < m(\pi^+\mu^+\mu^-) < 2.4$ GeV/c^2. We observe 51 events in the D_s^+ signal region 1.91 GeV/c^2

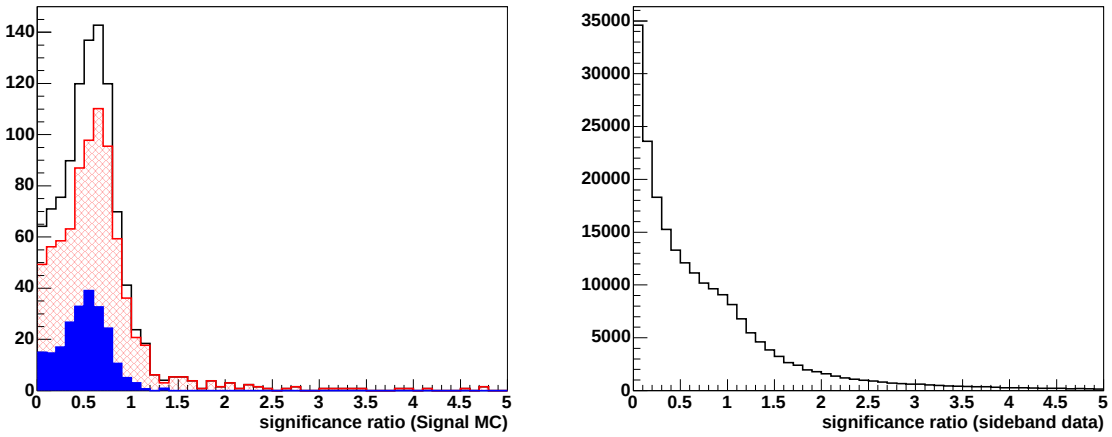

FIG. 9: The significance ratio variable, $\mathcal{R}_\mathcal{S}$. The distribution on the left is $D_s \to \phi\pi \to \pi\mu^+\mu^-$ signal MC (left). The hatched red histogram is the prompt component; the solid blue histogram is the $B \to D_s$ component; the open black histogram is the sum of the two components. The distribution on the right is D candidates in the 508 pb^{-1} data sample in the D mass sideband regions $1.4 < m(\pi\mu^+\mu^-) < 1.75$ GeV/c^2 and $2.05 < m(\pi\mu^+\mu^-) < 2.4$ GeV/c^2.

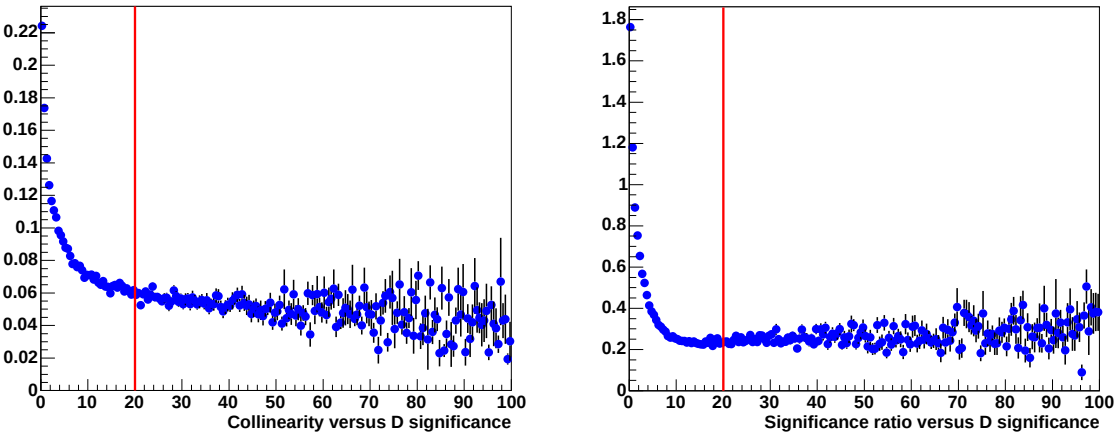

FIG. 10: Examples of correlations between the background suppression variables. In most cases, the multidimensional phase space can be split into correlated and uncorrelated regions as indicated above by the line at $\mathcal{S}_D = 20$.

$< m(\pi^+\mu^+\mu^-) < 2.03$ GeV/c^2 with an expected background of 18 events determined from extrapolating the event yields in the sidebands. This gives an excess of 33 events with a significance above background of 7.8 standard deviations.

The $D^+ \to \phi\pi^+ \to \pi^+\mu^+\mu^-$ signal is extracted from a binned likelihood fit to the data sample with $d > 0.9$ shown in Fig. 12 assuming possible contributions from D_s^+ and D^+ initial states as signal and combinatoric background. The signal distributions are modeled as Gaussians. The parameters are determined by relaxing the requirement on d to $d > 0.75$ and floating the mean and sigma of the D_s^+ Gaussian. The difference in the means of the D_s^+ and D^+ Gaussians are constrained to the known mass difference [14] and the sigmas are constrained by $\sigma(D^+) = (m(D^+)/m(D_s^+)) \times \sigma(D_s^+)$. The background is modeled as an exponential. The final fit on this loose data set contains six free parameters: the three normalizations for the D_s^+, D^+, and background contributions, the mean and sigma for the D_s^+ Gaussian, and the slope of the background. The results of the fit are displayed in Fig 13. The fit yields 56^{+12}_{-11} D_s^+ candidates in the region $d > 0.75$. The parameters of the fit agree well with the values expected from MC.

Using the Gaussian parameters determined above, we search for an excess of D^+ events in the $d > 0.9$ data sample. The fit parameterization is identical to the fit above with the exception that the D_s^+ mean and sigma are now fixed to the values determined in the fit to the $d > 0.75$ region. The free parameters in the fit are the three normalizations and

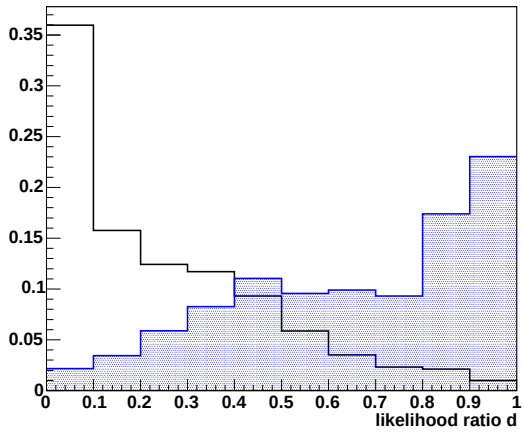

FIG. 11: Likelihood ratio separating signal from background. The blue hatched histogram is $D_s \to \phi\pi \to \pi\mu^+\mu^-$ signal MC. The open histogram is D candidates in the 508 pb^{-1} data sample in the D mass sideband regions $1.4 < m(\pi\mu^+\mu^-) < 1.75$ GeV/c^2 and $2.05 < m(\pi\mu^+\mu^-) < 2.4$ GeV/c^2.

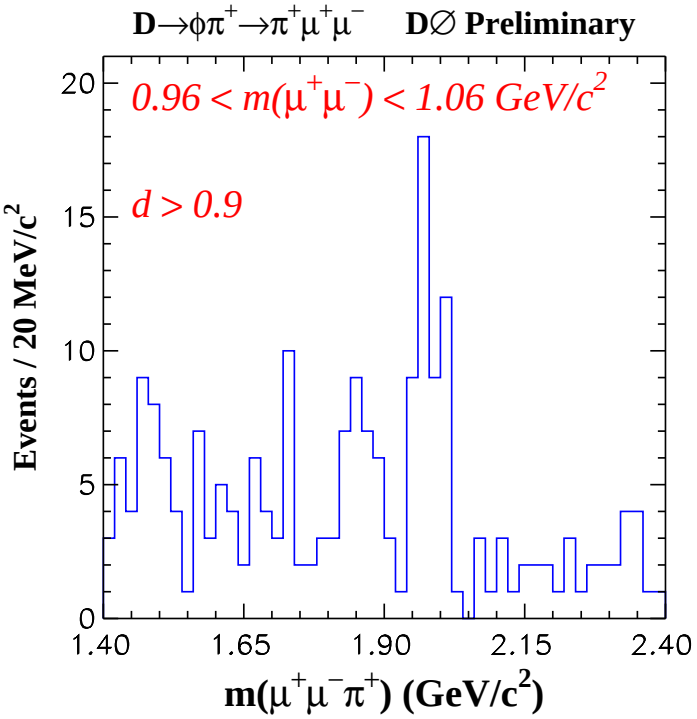

FIG. 12: The $m(\pi^+\mu^+\mu^-)$ invariant mass spectrum for candidate events in the region $0.96 < m(\mu^+\mu^-) < 1.06$ GeV/c^2 and likelihood ratio $d > 0.9$.

the slope of the background. The results of the fit are also displayed in Fig. 13. The fit yields $13.2^{+5.6}_{-4.9}$ D^+ candidates in the region $d > 0.9$. To reduce the effect of statistical fluctuations this D^+ yield obtained from the fit to the $d > 0.9$ sample is normalized using the D_s^+ yield in the $d > 0.75$ sample.

The systematic error in the ratio signal yields are determined by varying the fit parameters by $\pm 1\sigma$, using double Gaussian parameterizations for the signal distributions with parameters fixed to the expected values, parameterizing the background as a second order polynomial instead of an exponential, and shifting the binning by half the bin width. Adding the deviations in quadrature gives an error on the ratio of D^+ to D_s^+ yields of $+14\%$ and -24%.

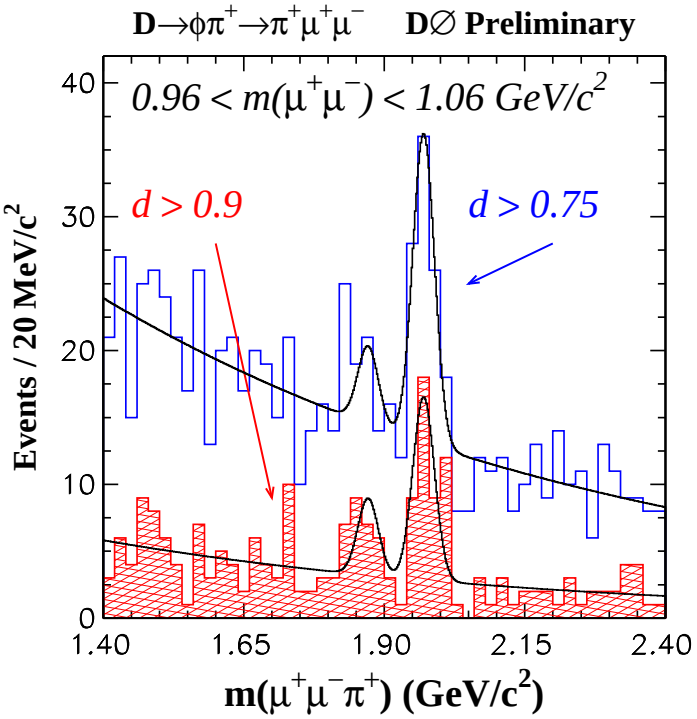

FIG. 13: The $m(\pi^+\mu^+\mu^-)$ mass spectrum for events with the likelihood ratio requirement $d > 0.75$ (blue) and $d > 0.9$ (red hatched). The results of binned likelihood fits to the distributions including contributions for D_s^+, D^+, and combinatoric background are overlaid on the histograms.

The significance in the D^+ yield is determined based on the change in the fit likelihood between when the D^+ yield is a free parameter and when it is constrained to zero. To account for systematic effects, we quote the lowest value obtained when varying the fitting functions as discussed above. The significance indicates that the D^+ excess is consistent with a 2.7σ fluctuation in the background. The fluctuation hypothesis is further supported by the fit to the $d > 0.75$ data sample that indicates no increase in the D^+ yield for a much higher efficiency.

RESULTS

Applying an efficiency correction for the different d requirements, and correcting for the production fractions of D_s^+ to D^+ mesons gives

$$\mathcal{B}(D^+ \to \phi\pi^+ \to \pi^+\mu^+\mu^-) = \frac{f(D_s^+)}{f(D^+)} \times \frac{\epsilon(D_s^+; d > 0.75)}{\epsilon(D^+; d > 0.9)} \times \frac{N(D^+; d > 0.9)}{N(D_s^+; d > 0.75)} \times \mathcal{B}(D_s^+ \to \phi\pi^+) \times \mathcal{B}(\phi \to \mu^+\mu^-).$$

The production fractions are $f(D_s^+) = 0.101 \pm 0.027$ and $f(D^+) = 0.232 \pm 0.018$ [15]. The efficiency ratio determined from MC is 1.6 ± 0.3 where the error is determined by comparing the expected and measured yields of D_s^+ events in the $d > 0.9$ sample compared to the $d > 0.75$ sample. The D_s^+ yield as a function of d is displayed in Fig. 14. The systematic error on the efficiency ratio was also tested by scanning the ratio as a function of variables that are most likely to disagree between MC and data such as the D_s p_T, tracking resolution, and event multiplicity. The efficiency ratio was found to be stable within the quoted error.

The D_s^+ and ϕ branching fractions are taken from [14]. Combining the above quantities yields a ratio of branching fractions of

$$\frac{\mathcal{B}(D^+ \to \phi\pi^+ \to \pi^+\mu^+\mu^-)}{\mathcal{B}(D_s^+ \to \phi\pi^+ \to \pi^+\mu^+\mu^-)} = 0.17^{+0.08\ +0.06}_{-0.07\ -0.07}$$

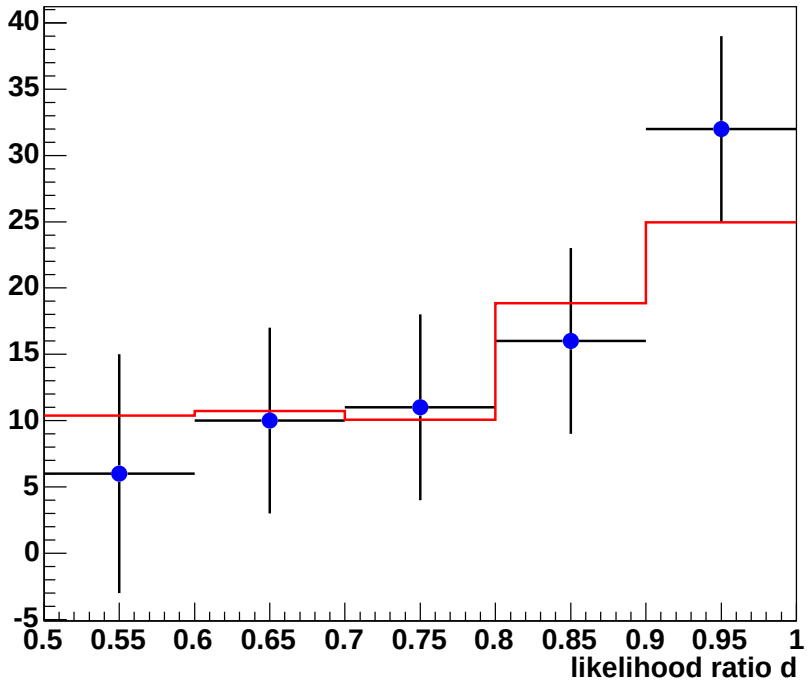

FIG. 14: The $D_s^+ \to \phi\pi^+ \to \pi^+\mu^+\mu^-$ yield as a function of the likelihood ratio d. The points with errors are the D_s yields to fits of the $m(\pi^+\mu^+\mu^-)$ distribution in exclusive bins of d. The histogram is the d distribution for D_s^+ signal MC. The two distributions are normalized to the same area.

and a branching fraction of

$$\mathcal{B}(D^+ \to \phi\pi^+ \to \pi^+\mu^+\mu^-) = (1.70^{+0.79\ +0.76}_{-0.73\ -0.82}) \times 10^{-6}.$$

The sources of error are listed in Table I.

We determine the upper limit by integrating the likelihood to

$$\frac{\int_0^{UL} dr\mathcal{L}(r)}{\int_0^{\infty} dr\mathcal{L}(r)} = 0.9,$$

where $r = N(D^+; d > 0.9)/N(D_s^+; d > 0.75)$. The likelihood is assumed to be Gaussian with a sigma taken as the statistical and systematic errors added in quadrature. This leads to

$$\frac{\mathcal{B}(D^+ \to \phi\pi^+ \to \pi^+\mu^+\mu^-)}{\mathcal{B}(D_s^+ \to \phi\pi^+ \to \pi^+\mu^+\mu^-)} < 0.28 \ \ (90\% \ \ \text{C.L.})$$

and

$$\mathcal{B}(D^+ \to \phi\pi^+ \to \pi^+\mu^+\mu^-) < 3.14 \times 10^{-6} \ \ (90\% \ \ \text{C.L.}).$$

CONCLUSIONS

In conclusion, we have clearly observed the $D_s^+ \to \phi\pi^+ \to \pi^+\mu^+\mu^-$ process indicating that we have achieved better sensitivity to three body FCNC charm meson decays than any previous experiment that has reported results on these modes. Our SM limit on the $D^+ \to \phi\pi^+ \to \pi^+\mu^+\mu^-$ is almost a factor of 3 below the previous best limit set by the FOCUS collaboration [7]. This constitutes the first step in the program to search for new phenomena in FCNC charm

TABLE I: Sources of error. The errors on the $D_s^+ \to \phi\pi^+$ and $\phi \to \mu^+\mu^-$ branching fractions only contribute to the absolute $D^+ \to \phi\pi^+ \to \pi^+\mu^+\mu^-$ upper limit.

	error (%)
statistics	$+47, -43$
fitting	$+14, -24$
$f(D_s^+)$	26
$f(D^+)$	8
$\epsilon(D_s^+)/\epsilon(D^+)$	19
$\mathcal{B}(D_s^+ \to \phi\pi^+)$	25
$\mathcal{B}(\phi \to \mu^+\mu^-)$	7

decays that will be followed by a search for an excess in events outside the ϕ mass region of the $m(\mu^+\mu^-)$ spectrum as well as a model independent limit of $d\Gamma/dm(\mu^+\mu^-)$.

We thank the staffs at Fermilab and collaborating institutions, and acknowledge support from the Department of Energy and National Science Foundation (USA), Commissariat à L'Energie Atomique and CNRS/Institut National de Physique Nucléaire et de Physique des Particules (France), Ministry for Science and Technology and Ministry for Atomic Energy (Russia), CAPES, CNPq and FAPERJ (Brazil), Departments of Atomic Energy and Science and Education (India), Colciencias (Colombia), CONACyT (Mexico), Ministry of Education and KOSEF (Korea), CONICET and UBACyT (Argentina), The Foundation for Fundamental Research on Matter (The Netherlands), PPARC (United Kingdom), Ministry of Education (Czech Republic), A.P. Sloan Foundation, Civilian Research and Development Foundation, Research Corporation, Texas Advanced Research Program, and the Alexander von Humboldt Foundation.

[1] A.L. Kagen and M. Neubert, Eur. Phys. J. C**7**, 5 (1999).
[2] A. Ali, E. Lunghi, C. Greb, G. Hiller, Phys. Rev. D**66**, 034002 (2002).
[3] K. Agashe and M. Graesser, Phys. Rev. D**54**, 4445 (1996).
[4] The inclusion of charge conjugate modes is implied throughout the text.
[5] G. Burdman, E. Golowich, J. Hewett, S. Pakvasa, Phys. Rev. D**66**, 014009 (2002).
[6] S. Fajfer, S. Prelovsek , P. Singer, Phys. Rev. D**64**, 114009 (2001).
[7] J. M. Link *et al.*, (FOCUS Collaboration), Phys. Lett. B**572**, 21 (2003).
[8] L. Babukhadia for the DØ Collaboration, FERMILAB-CONF-02/239-E, ICHEP 2002 proceedings, 906 (2002).
[9] T. Sjostrand, P. Eden, C. Friberg, L. Lonnblad, G. Miu, S. Mrenna and E. Norrbin, Computer Phys. Commun. 135, 238 (2001).
[10] D. J. Lange, Nuc. Inst. Meth. A**462**, 152 (2001).
[11] D. Acosta *et al.*, (CDF Collaboration), Phys. Rev. Lett. **91**, 241804 (2003).
[12] R. Brun, F. Bruyant, M. Maire, A. C. McPherson, P. Zanarini, CERN DD/EE/84-1 (1987).
[13] All charged particles in the event are clustered into jets using the DURHAM clustering algorithm with the p_T cut-off parameter 15 GeV/c. S. Catani, Yu. L .Dokshitzer, M. Olsson, G. Turnock, B.R. Webber, Phys.Lett. **B269**, 432 (1991).
[14] S. Eidelman *et al.*, (Particle Data Group), Phys. Lett. **B592**, 1 (2004).
[15] L. Gladilin, hep-ex/9912064 (1999).